

# High density of states in the pseudogap phase of the cuprate superconductor $\text{HgBa}_2\text{CuO}_{4+\delta}$ from low-temperature normal-state specific heat

C. Girod,<sup>1,2</sup> A. Legros,<sup>2,3</sup> A. Forget,<sup>3</sup> D. Colson,<sup>3</sup> C. Marcenat,<sup>4</sup>  
A. Demuer,<sup>5</sup> D. LeBoeuf,<sup>5</sup> L. Taillefer,<sup>2,6,\*</sup> and T. Klein<sup>1,†</sup>

<sup>1</sup>*Univ. Grenoble Alpes, CNRS, Grenoble INP, Institut Néel, F-38000 Grenoble, France*

<sup>2</sup>*Institut Quantique, Département de physique & RQMP,*

*Université de Sherbrooke, Sherbrooke, Québec J1K 2R1, Canada*

<sup>3</sup>*SPEC, CEA, CNRS-UMR3680, Université Paris-Saclay, Gif-sur-Yvette Cedex 91191, France*

<sup>4</sup>*Univ. Grenoble Alpes, CEA, IRIG, PHELIQS, LATEQS, F-38000 Grenoble, France*

<sup>5</sup>*Univ. Grenoble Alpes, INSA Toulouse, Univ. Toulouse Paul Sabatier, CNRS, LNCMI, F-38000 Grenoble, France*

<sup>6</sup>*Canadian Institute for Advanced Research, Toronto, Ontario M5G 1Z8, Canada*

(Dated: April 9, 2020)

The specific heat  $C$  of the single-layer cuprate superconductor  $\text{HgBa}_2\text{CuO}_{4+\delta}$  was measured in an underdoped crystal with  $T_c = 72$  K at temperatures down to 2 K in magnetic fields up to 35 T, a field large enough to suppress superconductivity at that doping ( $p \simeq 0.09$ ). In the normal state at  $H = 35$  T, a residual linear term of magnitude  $\gamma = 12 \pm 2$  mJ/K<sup>2</sup>mol is observed in  $C/T$  as  $T \rightarrow 0$ , a direct measure of the electronic density of states. This high value of  $\gamma$  has two major implications. First, it is significantly larger than the value measured in overdoped cuprates outside the pseudogap phase ( $p > p^*$ ), such as  $\text{La}_{2-x}\text{Sr}_x\text{CuO}_4$  and  $\text{Tl}_2\text{Ba}_2\text{CuO}_{6+\delta}$  at  $p \simeq 0.3$ , where  $\gamma \simeq 7$  mJ/K<sup>2</sup>mol. Given that the pseudogap causes a loss of density of states, and assuming that  $\text{HgBa}_2\text{CuO}_{4+\delta}$  has the same  $\gamma$  value as other cuprates at  $p \simeq 0.3$ , this implies that  $\gamma$  in  $\text{HgBa}_2\text{CuO}_{4+\delta}$  must peak between  $p \simeq 0.09$  and  $p \simeq 0.3$ , namely at (or near) the critical doping  $p^*$  where the pseudogap phase is expected to end ( $p^* \simeq 0.2$ ). Secondly, the high  $\gamma$  value implies that the Fermi surface must consist of more than the single electron-like pocket detected by quantum oscillations in  $\text{HgBa}_2\text{CuO}_{4+\delta}$  at  $p \simeq 0.09$ , whose effective mass  $m^* = 2.7 m_0$  yields only  $\gamma = 4.0$  mJ/K<sup>2</sup>mol. This missing mass imposes a revision of the current scenario for how pseudogap and charge order respectively transform and reconstruct the Fermi surface of cuprates.

## I. INTRODUCTION

Despite three decades of intense research, fundamental questions remain about the phase diagram of cuprate superconductors [1]. The central enigma is the nature of the pseudogap phase, an elusive phase that exists below a temperature  $T^*$  and below a critical hole concentration (doping)  $p^*$  (Fig. 1), whose defining characteristic is a drop in the electronic density of states (DOS) [2]. To crack this enigma, a crucial piece of information is the Fermi surface in the ground state of the pseudogap phase, at  $T = 0$  without superconductivity, and the associated DOS. This kind of information has only recently begun to surface [3], but the picture is still far from complete.

Well above  $p^*$ , cuprates are fairly conventional metals with a well characterized Fermi surface, namely a large quasi-2D cylinder, in agreement with band structure calculations. In the single-layer material  $\text{Tl}_2\text{Ba}_2\text{CuO}_{6+\delta}$  (Tl2201), this is established by angle-resolved photoemission (ARPES) [4] and angle-dependent magnetoresistance (ADMR) [5] measurements, and quantum oscillations [6, 7]. The measured cross-sectional area of the Fermi surface yields a carrier density (per Cu atom)  $n = 1 + p$ . The quantum oscillations also provide a measure of the carrier effective mass  $m^*$ , whose value at  $p = 0.29 \pm 0.02$  is  $m^* = 5.2 \pm 0.4 m_0$  [7]. Converting  $m^*$  to a specific heat coefficient  $\gamma$  ( $= C/T$  at  $T \rightarrow 0$ ), via the relation  $\gamma = 1.49 (m^*/m_0)$  (in

mJ/K<sup>2</sup>mol), yields  $\gamma = 7.6 \pm 0.6$  mJ/K<sup>2</sup>mol [7], in agreement with the specific heat measured directly on a non-superconducting sample at  $p = 0.33 \pm 0.02$ , where  $\gamma = 6.5 \pm 1.0$  mJ/K<sup>2</sup>mol [8]. The data in Tl2201 are in excellent agreement with the two other cuprates whose specific heat has been measured at  $p \simeq 0.3$ , namely  $\text{La}_{2-x}\text{Sr}_x\text{CuO}_4$  (LSCO), where  $\gamma = 6.9 \pm 0.7$  mJ/K<sup>2</sup>mol at  $p = 0.33$  [9] and  $\text{La}_{1.6-x}\text{Nd}_{0.4}\text{Sr}_x\text{CuO}_4$  (Nd-LSCO), where  $\gamma = 6.5 \pm 1.0$  mJ/K<sup>2</sup>mol at  $p = 0.36$  [3]. In summary,  $\gamma \simeq 7$  mJ/K<sup>2</sup>mol at  $p \simeq 0.3$ , a doping well above  $p^*$  in all cases. (Note that this value is 3 times larger than the value calculated from LDA band structure, reflecting a significant mass enhancement due to electron correlations not captured by the calculations.)

The key question is what happens to that simple Fermi surface when doping is reduced below  $p^*$ . It is clearly transformed, but we still do not know exactly how. ARPES studies on various cuprates show that states near  $(\pi, 0)$  are gapped [11], leaving only 'Fermi arcs' at nodal locations in  $k$ -space, also seen by scanning tunnelling spectroscopy (STM) in  $\text{Ba}_2\text{Sr}_2\text{CaCu}_2\text{O}_8$  (Bi2212) [12]. Hall effect measurements on  $\text{YBa}_2\text{Cu}_3\text{O}_y$  (YBCO) [13], Nd-LSCO [14] and Tl2201 [15] show a large drop in the Hall number  $n_H$ , from  $n_H \simeq 1 + p$  above  $p^*$  to  $n_H \simeq p$  below  $p^*$ , attributed to a drop in carrier density, also detected in thermal conductivity [16]. It is tempting to interpret these various signatures in terms of a Fermi surface consisting of four small closed nodal hole pockets

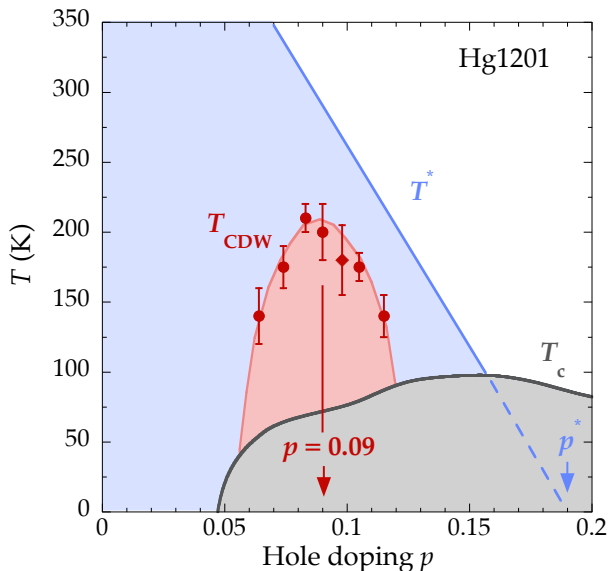


FIG. 1. Temperature-doping phase diagram of Hg1201, showing the superconducting transition temperature  $T_c$  (grey line), the pseudogap temperature  $T^*$  (blue line), and the onset temperature for charge-density-wave (CDW) modulations seen by resonant x-ray scattering (red circles) from Ref. 10 and references therein. The red vertical arrow indicates the doping of our sample ( $p \simeq 0.09$ ), and the blue vertical arrow marks the pseudogap critical point  $p^*$ , where  $T^*$  extrapolates to zero.

containing a total of  $p$  holes, one side of which is detected as an arc in ARPES and STM. But that remains to be demonstrated.

Associated with the Fermi surface transformation across  $p^*$  is a 10-fold drop in the DOS below  $p^*$ , first detected as a rapid reduction in the magnitude of the specific heat jump at  $T_c$  in YBCO [17]. It appeared as though the opening of the pseudogap causes a loss of DOS. Recently, a direct measurement of the normal-state specific heat at  $T \rightarrow 0$  in Nd-LSCO and  $\text{La}_{1.8-x}\text{Eu}_{0.2}\text{Sr}_x\text{CuO}_4$  (Eu-LSCO) has suggested a different paradigm: before the DOS drops below  $p^*$ , it first rises as  $p \rightarrow p^*$  from above. In other words, the DOS above and below  $p^*$  is more or less the same, but it goes through a large peak in between, at  $p^*$ . Indeed in Nd-LSCO, where  $p^* = 0.23$ ,  $\gamma \simeq 5$  mJ/K<sup>2</sup>mol both at  $p = 0.07$  and at  $p = 0.40$ , but  $\gamma \simeq 22$  mJ/K<sup>2</sup>mol at  $p = 0.24$  [3]. This peak displays the classic thermodynamic signature of quantum criticality, whereby  $C/T \propto -\log(1/T)$  at  $p^*$  [3]. The Fermi surface transformation at  $p^*$  is therefore associated with a quantum critical point, whose nature is as yet unknown. Seen so far only in Nd-LSCO [3] and LSCO [18], it is important to establish whether a peak in  $C$  vs  $p$  at  $p^*$ , at  $T \rightarrow 0$ , is a generic property of cuprates.

In this Article, we explore this question with measurements of the specific heat in the cuprate material

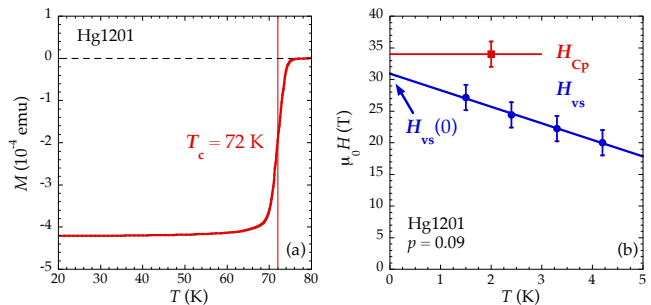


FIG. 2. (a) Zero-field cooled SQUID magnetization curve for our Hg1201 sample as a function of temperature, displaying a sharp superconducting transition at  $T_c = 72 \pm 2$  K, defined as the midpoint of the transition. (b) Temperature dependence of the irreversibility field  $H_{vs}(T)$  (blue circles), deduced from resistivity measurements on a sample of Hg1201 with  $T_c = 72$  K [19]. The vortex solid line extrapolates linearly to  $H_{vs} = 31 \pm 2$  T (blue line), in agreement with the field above which the specific heat saturates at  $T = 2$  K,  $H_{Cp} = 34 \pm 2$  T (red square and line). This shows that our sample has a doping very similar to the doping at which quantum oscillations have been detected.

$\text{HgBa}_2\text{CuO}_{4+\delta}$  (Hg1201), at a doping  $p \simeq 0.09$ , well below  $p^* \simeq 0.2$  (Fig. 1). By applying a magnetic field of 35 T to suppress superconductivity, we access directly the normal-state  $C(T)$  at low  $T$ , and find a linear term  $\gamma = 12 \pm 2$  mJ/K<sup>2</sup>mol. This is much larger than the value found in all other cuprates at  $p \simeq 0.3 > p^*$ . If we require that the pseudogap in Hg1201 also causes a drop in DOS below  $p^*$ , and assume that Hg1201 has the same  $\gamma$  value as other cuprates at  $p \simeq 0.3$ , then  $C$  must peak at  $p^*$ . The very large  $\gamma$  value we observe in Hg1201 also implies that the Fermi surface at  $p \simeq 0.09$  includes more pieces than the one small pocket detected by quantum oscillations [19, 20], forcing a revision of the current scenario of Fermi-surface reconstruction by charge order [20, 21].

## II. METHODS

Our single crystal of Hg1201 was grown using a self-flux technique [22]. Its mass is  $m \simeq 1.1$  mg. It was annealed in a vacuum of  $3 \times 10^{-1}$  mbar at 275 °C during 67 hours, to produce a superconducting transition temperature  $T_c = 72$  K, defined as the mid-point of the drop in magnetization measured in a SQUID magnetometer, with a field of 10 Oe (see Fig. 2a). The estimated hole concentration (doping) for such a  $T_c$  value is  $p \simeq 0.09$  (Fig. 1).

The specific heat was measured using an AC microcalorimetry technique described in Ref. 3. The total heat capacity,  $C$ , was obtained through the equation  $C = P_{ac} \sin(-\phi)/2\omega|T_{ac}|$ , where  $P_{ac}$  is a periodically modulated heating power,  $\phi$  is the thermal phase shift and  $T_{ac}$  the induced temperature oscillations. A minia-

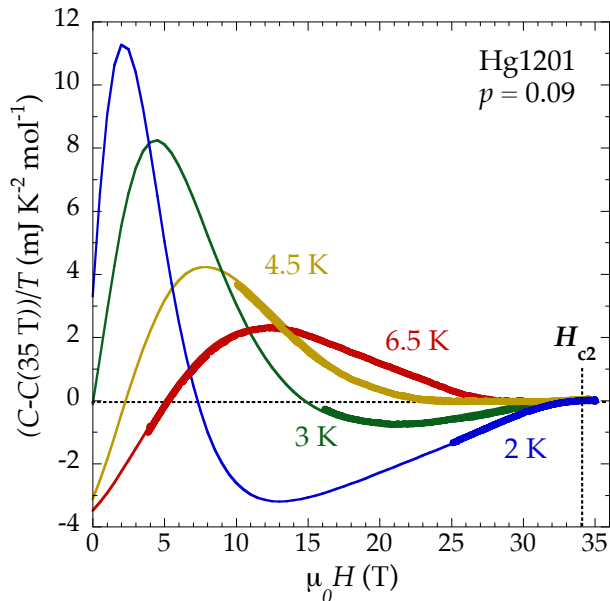


FIG. 3. Specific heat  $C$  of our Hg1201 sample as a function of magnetic field  $H$ , plotted as  $C/T$  vs  $H$ , for four temperatures as indicated. A constant term is subtracted from each isotherm, namely the value of  $C/T$  at  $H = 35$  T, which is plotted in Fig. 4. The vertical dashed line marks the upper critical field  $H_{C_p} = 34 \pm 2$  T, defined as the field above which  $C$  vs  $H$  has saturated. The thin lines indicate for each temperature the field dependence expected for a standard two level Schottky contribution with a gap varying as  $\Delta/k_B = 2.5 + 1.2 \times H$ , on top of a linear field dependence of the electronic specific heat in the superconducting state (up to 25 T).

ture Cernox resistive chip was split into two parts and attached to a small copper ring with PtW(7%) wires. The first half was used as the heater delivering  $P_{ac}$  and the second half was used to record the temperature  $T_{ac}$ . In order to subtract the heat capacity of the sample mount (chip + a few  $\mu\text{g}$  of Apiezon grease used to glue the sample onto the back of the chip), the empty chip (with grease) was measured prior to the sample measurements. A precise *in situ* calibration and corrections of the thermometers in magnetic field were included in the data treatment. This technique enabled us to obtain the absolute value of the specific heat of miniature single crystals with an accuracy better than  $\sim 5\%$  below 10 K, as checked from measurements on ultrapure copper [3].

A magnetic field was applied normal to the  $\text{CuO}_2$  planes (along the  $c$  axis) to suppress superconductivity. The zero temperature upper critical field  $H_{c2}$  can be obtained from resistance measurements of the vortex-solid field  $H_{vs}(T)$ , defined as the field below which the sample resistance is zero [23]. By extrapolating  $H_{vs}(T)$  to  $T \rightarrow 0$ , we get  $H_{c2} = H_{vs}(0)$ . From the data of Ref. 19, on a sample of Hg1201 with a very similar  $T_c$  ( $= 72$  K), we find  $H_{c2} = 31 \pm 2$  T (Fig. 2b). We shall see that this is nicely consistent with the  $H_{c2}$  value obtained

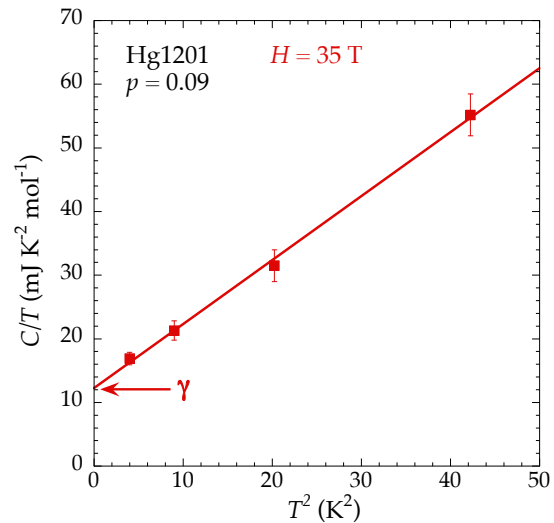


FIG. 4. Normal-state specific heat at  $H = 35$  T, for the four isotherms of Fig. 3, plotted as  $C/T$  vs  $T^2$  (red squares). The solid red line is a linear fit of the four data points to  $C/T = \gamma + \beta T^2$ , giving  $\gamma = 12 \pm 2$  mJ/K<sup>2</sup>mol and  $\beta = 1.0 \pm 0.1$  mJ/K<sup>4</sup>mol.

from the saturation of  $C$  vs  $H$  in our own sample *i.e.*  $H_{c2} \approx H_{C_p} = 34 \pm 2$  T (Fig. 2b). Given that  $H_{c2}$  varies rapidly with  $p$  near  $p = 0.1$  (in YBCO and presumably also in Hg1201), this matching of  $H_{c2}$  and  $T_c$  values confirms that our specific heat data and the quantum oscillation data of Ref. 19 are being compared at the same doping.

### III. RESULTS

In Fig. 3, we show the specific heat  $C$  of our Hg1201 sample, plotted as  $C/T$  vs  $H$ , at 4 different temperatures:  $T = 2.0, 3.0, 4.5,$  and  $6.5$  K. For clarity, the data have been shifted to zero at 35 T by subtracting the value of  $C/T$  at  $H = 35$  T, which is itself plotted in Fig. 4. In Fig. 3, a Schottky anomaly is clearly visible below  $\sim 30$  T for the highest temperature (6.5 K). This Schottky contribution can be well described by the standard expression  $C_{\text{Schottky}} \propto (\Delta/k_B T)^2 \exp(\Delta/k_B T)/(1 + \exp(\Delta/k_B T))^2$  with  $\Delta/k_B \approx 2.5 + 1.2 \times H$  (K) (thin solid lines in Fig. 3), in agreement with the gap value previously inferred by Kemper [24]. As expected, this Schottky contribution moves progressively to lower fields with decreasing temperature. At  $T = 4.5$  K, it is negligible above 25 T and at our base temperature of 2 K, the data are free of Schottky contribution above 25 T. At  $T = 2$  K, the increase in  $C/T$  vs  $H$  reflects the suppression of superconductivity, which is complete by 35 T;  $C/T$  vs  $H$  has reached saturation for fields above  $H_{C_p} = 34 \pm 2$  T. The value of  $C/T$  at  $H = 35$  T is therefore the normal-state value, free of any Schottky contribution, plotted as

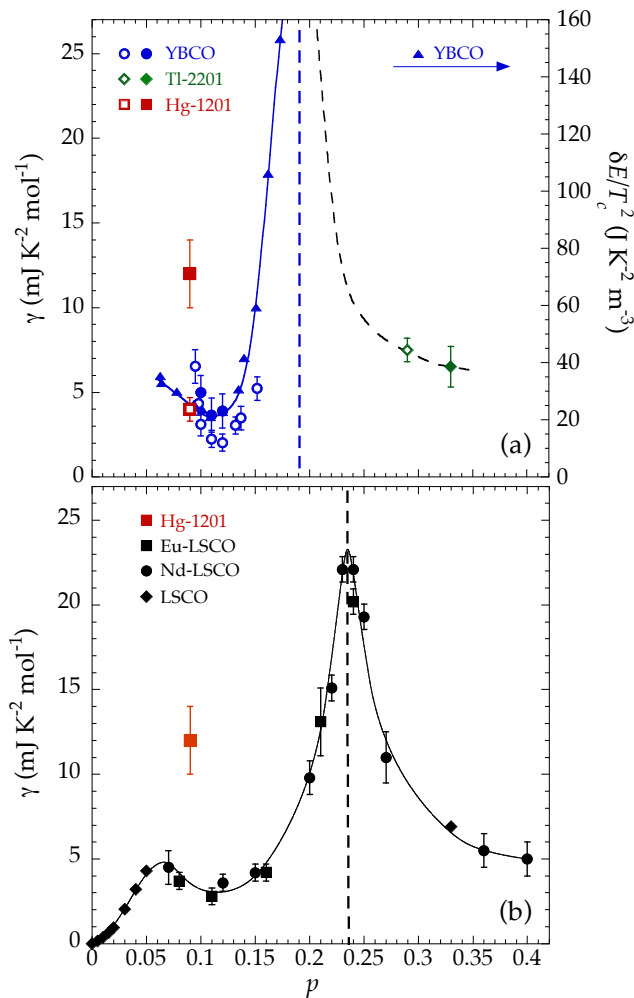


FIG. 5. (a) Normal-state specific heat coefficient  $\gamma$  ( $= C/T$  at  $T \rightarrow 0$ ) in three hole-doped cuprates: Hg1201 at  $p \simeq 0.09$  (red square, left axis, from Fig. 4); YBCO at  $p = 0.10, 0.11$  and  $0.12$  (solid blue circles, left axis [25]); non-superconducting Tl2201 at  $p = 0.33 \pm 0.02$  (solid green diamond, left axis [8]). Also shown are the values of  $\gamma$  obtained from the effective mass  $m^*$  measured by quantum oscillations (Eq. 1) in Hg1201 at  $p \simeq 0.09$  (open red square, left axis [20]); YBCO at  $0.08 < p < 0.16$  (open blue circles, left axis [26, 27]); Tl2201 at  $p = 0.29 \pm 0.02$  (open green diamond, left axis [7]). The units for  $C$  are expressed per mole of planar Cu. The blue solid line is a guide to the eye. The blue dashed line marks the pseudogap critical point  $p^*$  in YBCO. The black dashed line is a guide to the eye. (b) Normal-state specific heat coefficient  $\gamma$  in four hole-doped cuprates: Hg1201 at  $p \simeq 0.09$  (red square, from Fig. 4); LSCO (black diamonds) at  $p < 0.06$  [28] and at  $p = 0.33$  [9]; Nd-LSCO (black circles [3]); Eu-LSCO (black squares [3]). The data points at  $p = 0.20, 0.21, 0.22, 0.23, 0.24$  and  $0.25$  are not  $\gamma$  but rather  $C_{\text{el}}/T$  at  $T = 0.5$  K, where  $C_{\text{el}}$  is the normal-state electronic specific heat [3]. The black dashed line marks  $p^*$  in Nd-LSCO [3, 14].

$C/T$  vs  $T^2$  in Fig. 4.

The 35 T normal state data are well described by a linear fit,  $C/T = \gamma + \beta T^2$ , with  $\gamma = \gamma_N = 12 \pm 2$

Material	Doping	State	$\gamma$ ( $\text{mJ/K}^2 \text{mol}^{-1}$ )	Ref.
Hg1201	0.09	SR-CDW	$12 \pm 2$	this work
YBCO	0.10	LR-CDW	$5 \pm 1$	[25]
LSCO	0.10	CDW + SDW	$5 \pm 1$	[18]
Eu-LSCO	0.11	CDW + SDW	$2.8 \pm 0.5$	[3]
Nd-LSCO	0.12	CDW + SDW	$3.6 \pm 0.5$	[3]
LSCO	0.33	FL	$6.9 \pm 0.7$	[9]
Tl2201	0.33	FL	$6.5 \pm 1.0$	[8]
Nd-LSCO	0.36	FL	$6.5 \pm 1.0$	[3]

TABLE I. Residual linear term  $\gamma$  in the specific heat of various hole-doped cuprates, measured in the normal state as  $C/T$  in the limit  $T \rightarrow 0$ , both in the underdoped regime at  $p \simeq 0.1$  (top group) and in the strongly overdoped regime at  $p > 0.3$  (bottom group). The units for  $\gamma$  are expressed per Cu atom in the  $\text{CuO}_2$  planes. In the absence of superconductivity, the ground state is either long-range (LR) 3D CDW order (in YBCO), short-range (SR) CDW correlations (in Hg1201), combined CDW and SDW modulations (stripe order), or a Fermi liquid (at  $p > 0.3$ ).

$\text{mJ/K}^2 \text{mol}$  and  $\beta = 1.0 \pm 0.1 \text{ mJ/K}^4 \text{mol}$ , with error bars that combine the uncertainty on the absolute value of  $C$  and the uncertainty on the fit. Our values for  $\gamma$  and  $\beta$  are in excellent agreement with those previously obtained by Kemper on an underdoped crystal of Hg1201 with  $T_c = 72$  K [24]. Note that in a  $d$ -wave superconductor, a non-zero residual Sommerfeld coefficient  $\gamma_R$  is usually observed due to disorder-induced pair-breaking effects. The value of  $\gamma_R$  then strongly depends on disorder, and slight variations in the level of disorder from sample to sample will result in large variations in  $\gamma_R$ , as reported previously [24]. However, disorder does not affect the normal state  $\gamma_N$ , and our observation of the same large  $\gamma_N$  value in two separate studies confirms that it is an intrinsic electronic property of Hg1201.

## IV. DISCUSSION

In Fig. 5, we compare our value of  $\gamma$  in Hg1201 at  $p = 0.09$  to  $\gamma$  values previously measured in other hole-doped cuprates (in the normal state without superconductivity). The values reported so far at dopings close to  $p = 0.1$  are listed in Table I (where units are per mole of planar Cu). We see that  $\gamma$  in Hg1201 ( $12 \text{ mJ/K}^2 \text{mol}$ ) is significantly larger than in YBCO ( $5 \text{ mJ/K}^2 \text{mol}$ ) [25, 29], LSCO ( $5 \text{ mJ/K}^2 \text{mol}$ ) [18], Nd-LSCO ( $4 \text{ mJ/K}^2 \text{mol}$ ) [3], and Eu-LSCO ( $3 \text{ mJ/K}^2 \text{mol}$ ) [3].

### A. Fermi surface and CDW order

At  $p \simeq 0.1$ , various factors will affect the DOS in the normal state. First, the pseudogap reduces the DOS (see discussion below). Secondly, in all the former materials there is some form of charge-density-wave (CDW) order

(or correlations) at  $p \simeq 0.1$ , detected by x-ray diffraction in Hg1201 [10], YBCO [30, 31], LSCO [32], Nd-LSCO [33], and Eu-LSCO [34], amongst others [1]. This CDW order causes a reconstruction of the Fermi surface, detected as a change of sign in the Hall and Seebeck coefficients, from positive at high temperature to negative at low temperature, in Hg1201 [35], YBCO [36–38], LSCO [39], Nd-LSCO [40], and Eu-LSCO [41]. This reconstruction reduces the DOS further, beyond the effect of the pseudogap, as indicated by the fact that  $\gamma$  vs  $p$  has a local minimum at  $p \simeq 0.12$  in YBCO [25], LSCO [18], Nd-LSCO [3], and Eu-LSCO [3], where CDW order is strongest. There is also a local minimum in the upper critical field,  $H_{c2}$  vs  $p$ , and in the associated condensation energy [23].

In YBCO, at the high fields used to access the normal-state  $\gamma$  ( $H > 25$  T), there is a long-range, unidirectional 3D CDW order [42, 43], not observed so far in any other cuprate. In particular, this long-range 3D order has not been seen in Hg1201. Although the comparative impact on the Fermi surface and associated DOS of this 3D order *vs* the short-range 2D order is not yet clear, it is conceivable that the smaller  $\gamma$  value in YBCO (5 mJ/K<sup>2</sup>mol) *vs* Hg1201 (12 mJ/K<sup>2</sup>mol) has to do with the difference in their CDW ordering. (Note also that  $\gamma$  in YBCO rises fast below  $p = 0.11$  [25], and so will become larger than 5 mJ/K<sup>2</sup>mol at  $p < 0.10$ .)

A third factor that should affect the DOS of the normal state is spin order, which occurs in addition to charge order in LSCO, Nd-LSCO and Eu-LSCO, at  $p \simeq 0.1$  (*e.g.* [44]), but *not* in Hg1201 or YBCO [45]. Indeed, having spin order in addition to charge order is expected to modify the way in which the Fermi surface is reconstructed [46]. It is therefore conceivable that the larger  $\gamma$  value in Hg1201 (12 mJ/K<sup>2</sup>mol) *vs* LSCO (5 mJ/K<sup>2</sup>mol), Nd-LSCO (4 mJ/K<sup>2</sup>mol) or Eu-LSCO (3 mJ/K<sup>2</sup>mol), could be due to the presence of spin ordering in the latter materials.

A fourth factor that could affect the DOS is the proximity of a van Hove singularity. Such a singularity is present in hole-doped cuprates as the Fermi surface goes from hole-like to electron-like upon doping. However, ARPES data on Hg1201 [47] show that the van Hove singularity in Hg1201 is located at a doping well above optimal doping, in accordance with a tight binding model that predicts  $p_{\text{vHs}} \gg 0.19$ . (In Nd-LSCO,  $p_{\text{vHs}} \approx 0.23$  and yet a  $\gamma$  value as low as 4 mJ/K<sup>2</sup> mol is reported at  $p = 0.12$  [3].) Therefore, given that  $p_{\text{vHs}} \gg 0.09$  in Hg1201, we expect that the  $\gamma$  value measured at  $p = 0.09$  in Hg1201 is only slightly affected by the van Hove singularity, and the large value of 12 mJ/K<sup>2</sup> mol is certainly not the result of this singularity.

Our current knowledge of the Fermi surface of YBCO and Hg1201 comes mostly from quantum oscillations, detected in YBCO at dopings from  $p \simeq 0.09$  to  $p \simeq 0.15$  [26, 27, 48] and in Hg1201 at  $p \simeq 0.09$  [19, 20].

These oscillations provide a direct way to measure the effective mass  $m^*$ , for each (closed) piece of the Fermi surface. In 2D, a sum rule requires that the various values of  $m^*$  must add up to the specific heat  $\gamma$  [49]:

$$\gamma = \text{prefactor} \times \sum n_i (m_i/m_0) \quad , \quad (1)$$

where  $n_i$  is the number of equivalent pockets in the Brillouin zone,  $m_i$  is the mass  $m^*$  of each independent pocket,  $m_0$  is the electron mass, and the prefactor is equal to 1.47 for YBCO and 1.49 for Hg1201, when  $\gamma$  is expressed in mJ/K<sup>2</sup>mol (per mole of planar Cu).

In YBCO, at least 4 different frequencies have been resolved [50], the interpretation of which is still debated. At  $p = 0.10$ , the dominant frequency  $F = 530$  T has a mass  $m^* = 1.9 \pm 0.1 m_0$  [26, 27, 48], which yields  $\gamma = 1.47 \times 1.9 = 2.8 \pm 0.2$  mJ/K<sup>2</sup>mol (assuming one pocket per CuO<sub>2</sub> plane). This is significantly smaller than the measured  $\gamma = 5 \pm 1$  mJ/K<sup>2</sup>mol (Fig. 3a). Possible explanations for the missing mass include: the presence of a second closed pocket (with  $n_2 m_2 = 1.5 m_0$ ) [50]; the open band associated with the CuO chains of YBCO; an open piece of the Fermi surface associated with the CuO<sub>2</sub> planes.

In Hg1201, the situation is much simpler: there is only one CuO<sub>2</sub> plane per unit cell, no chains and only a single frequency is observed, giving  $F = 850$  T and  $m^* = 2.7 \pm 0.1 m_0$ , for a sample with  $T_c = 71$  K [20]. If this single frequency corresponds to one pocket per CuO<sub>2</sub> plane ( $n_1 = 1$ ), then  $\gamma = 1.49 \times 2.7 = 4.0 \pm 0.2$  mJ/K<sup>2</sup>mol. Similarly, in Ref. 19,  $F = 840$  T and  $m^* = 2.45 \pm 0.15 m_0$ , for a sample with  $T_c = 72$  K, giving  $\gamma = 3.7 \pm 0.2$  mJ/K<sup>2</sup>mol. (As discussed above in relation to Fig. 2b, with the same values of  $T_c$  and  $H_{c2}$ , our sample and the sample of ref. 19 have the very same doping). Having a value 3 times smaller than the measured  $\gamma$  then immediately implies that the Fermi surface of Hg1201 includes pieces beyond the small closed pocket that gives rise to the quantum oscillations. Therefore, the main scenario proposed so far for Hg1201 [20], whereby the Fermi surface consists of a single electron-like pocket per CuO<sub>2</sub> plane resulting from a reconstruction by biaxial CDW order [21], is ruled out.

The additional pieces of Fermi surface can either be other closed pockets, as yet undetected in quantum oscillation measurements, or open bands, undetectable in such measurements. If closed pockets, their total mass must be twice that of the measured mass ( $m^* = 2.7 m_0$ ). By comparison, in YBCO the total 'missing mass' is only 75% of the main mass ( $m^* = 1.9 m_0$ ). If open bands, these must represent a significant fraction of the total DOS. Note that open bands have been proposed in the context of a reconstruction by uniaxial CDW order [51]. Either way, a major rethinking of the Fermi surface of Hg1201 is necessary, and more generally of all underdoped cuprates.

## B. Pseudogap and peak in $\gamma$ vs $p$

Irrespective of what is the correct Fermi surface for Hg1201 at  $p \simeq 0.1$ , the striking fact remains that its measured  $\gamma$  (12 mJ/K<sup>2</sup>mol) is significantly larger than what is measured in the overdoped regime at  $p > 0.3$ , in various single-layer cuprates (Table I): Tl2201 (6.5 mJ/K<sup>2</sup>mol) [8]; LSCO (6.9 mJ/K<sup>2</sup>mol) [9]; Nd-LSCO (6.5 mJ/K<sup>2</sup>mol) [3]. How is that possible if the opening of the pseudogap below  $p^* \simeq 0.2$  (Fig. 1) causes a loss of DOS? A first explanation could be that this particular single-layer cuprate has a  $\gamma$  value for  $p > p^*$  much higher than the  $\gamma$  value measured in the other three single-layer cuprates at  $p = 0.3$ , i.e. LSCO, Nd-LSCO and Tl2201. However, we cannot think of any physical reason for that, in a regime where properties obey Fermi liquid theory and the Fermi surface is properly given by band structure calculations. A second, more natural explanation is that  $\gamma$  rises in going from  $p \simeq 0.3$  to  $p = p^*$ , and then drops in going from  $p = p^*$  to  $p \simeq 0.09$ , upon entering the pseudogap phase. In other words,  $\gamma$  peaks at  $p^*$ . Such a peak has been measured directly in both LSCO (with superconductivity removed by introduction of Zn impurities) [18] and in Nd-LSCO (with superconductivity removed by application of a magnetic field) [3].

In Nd-LSCO, the electronic specific heat  $C_{el}$  peaks sharply at  $p^* = 0.23$  (Fig. 3b). At  $p = 0.24$ ,  $C_{el}/T$  increases logarithmically as  $T \rightarrow 0$ , to reach  $C_{el}/T \simeq 21$  mJ/K<sup>2</sup>mol at  $T = 0.5$  K [3]. In YBCO, there are no direct measurements of the normal-state  $\gamma$  above  $p = 0.12$ , because the magnetic fields needed to suppress superconductivity when  $p > 0.12$  rapidly exceed 45 T [23]. It is nevertheless clear [2], from indirect measurements [17, 23], that the DOS increases dramatically in going from  $p = 0.12$  to  $p = p^* = 0.19$ . For example, in standard BCS theory,  $\gamma \propto \delta E/T_c^2$ , where  $\delta E$  is the condensation energy [2]. An estimate of  $\delta E$  in YBCO via measurements of the upper ( $H_{c2}$ ) and lower ( $H_{c1}$ ) critical fields, finds that  $\delta E/T_c^2$  increases by a factor 6.5 in going from  $p = 0.10$  to  $p = 0.18$  [23] (Fig. 3a). Given that  $\gamma = 5$  mJ/K<sup>2</sup>mol at  $p = 0.10$  (Table I), this implies that  $\gamma \simeq 35$  mJ/K<sup>2</sup>mol at  $p = p^*$  (Fig. 3a) – a value 3 times larger than  $\gamma$  in Hg1201 at  $p \simeq 0.09$  and 5 times larger than  $\gamma$  at  $p \simeq 0.33$ . We propose that if Hg1201 could be doped up to  $p \simeq 0.3$  and its normal-state  $\gamma$  could be measured across  $p^*$ , one would find that  $\gamma \simeq 7$  mJ/K<sup>2</sup>mol at  $p = 0.3$  and  $\gamma \simeq 30$  mJ/K<sup>2</sup>mol at  $p = p^*$ .

## V. CONCLUSION

By applying a magnetic field of 35 T to the single-layer cuprate Hg1201 at a doping  $p \simeq 0.09$ , we have suppressed its superconductivity and measured its normal-state specific heat  $C$ . Extrapolating  $C/T$  to  $T = 0$  yields  $\gamma = 12 \pm 2$  mJ/K<sup>2</sup>mol. This high value of  $\gamma$  has two ma-

ior implications. First, it is significantly larger than the value measured in overdoped cuprates outside the pseudogap phase, where  $\gamma \simeq 7$  mJ/K<sup>2</sup>mol. Given that the pseudogap causes a loss of density of states, this implies that  $\gamma$  must peak between  $p \simeq 0.1$  and  $p \simeq 0.3$ , namely at (or near) the critical doping  $p^*$  where the pseudogap phase is expected to end ( $p^* \simeq 0.2$ ) – as indeed found in LSCO and Nd-LSCO. Secondly, the high  $\gamma$  value implies that the Fermi surface of Hg1201 must consist of more than the single electron-like pocket detected by quantum oscillations in Hg1201 at  $p \simeq 0.09$ , whose effective mass yields only  $\gamma = 4.0 \pm 0.2$  mJ/K<sup>2</sup>mol. This missing mass imposes a revision of the current scenario for how pseudogap and charge order respectively transform and reconstruct the Fermi surface of cuprates.

## ACKNOWLEDGMENTS

L.T. acknowledges support from the Canadian Institute for Advanced Research (CIFAR) as a CIFAR Fellow and funding from the Natural Sciences and Engineering Research Council of Canada (NSERC; PIN:123817), the Fonds de recherche du Québec – Nature et Technologies (FRQNT), the Canada Foundation for Innovation (CFI), and a Canada Research Chair. This research was undertaken thanks in part to funding from the Canada First Research Excellence Fund. Part of this work was funded by the Gordon and Betty Moore Foundation's EPIQS Initiative (Grant GBMF5306 to L.T.).

---

\* louis.taillefer@usherbrooke.ca

† thierry.klein@neel.cnrs.fr

- [1] B. Keimer, S. A. Kivelson, M. R. Norman, S. Uchida, and J. Zaanen, *Nature* **518**, 179 (2015).
- [2] C. Proust and L. Taillefer, *Annual Review of Condensed Matter Physics* **10**, 409 (2019).
- [3] B. Michon, C. Girod, S. Badoux, J. Kačmarčík, Q. Ma, M. Dragomir, H. A. Dabkowska, B. D. Gaulin, J.-S. Zhou, S. Pyon, T. Takayama, H. Takagi, S. Verret, N. Doiron-Leyraud, C. Marcenat, L. Taillefer, and T. Klein, *Nature* **567**, 281 (2019).
- [4] D. C. Peets, J. D. F. Mottershead, B. Wu, I. S. Elfimov, R. Liang, W. N. Hardy, D. A. Bonn, M. Raudsepp, N. J. C. Ingle, and A. Damascelli, *New Journal of Physics* **9**, 28 (2007).
- [5] N. E. Hussey, M. Abdel-Jawad, A. Carrington, A. P. Mackenzie, and L. Balicas, *Nature* **425**, 814 (2003).
- [6] B. Vignolle, A. Carrington, R. A. Cooper, M. M. J. French, A. P. Mackenzie, C. Jaudet, D. Vignolles, C. Proust, and N. E. Hussey, *Nature* **455**, 952 (2008).
- [7] A. F. Bangura, P. M. C. Rourke, T. M. Benseman, M. Matusiak, J. R. Cooper, N. E. Hussey, and A. Carrington, *Physical Review B* **82**, 140501 (2010).
- [8] J. Wade, J. Loram, K. Mirza, J. Cooper, and J. Tallon, *Journal of Superconductivity* **7**, 261 (1994).

- [9] S. Nakamae, K. Behnia, N. Mangkorntong, M. Nohara, H. Takagi, S. J. C. Yates, and N. E. Hussey, *Physical Review B* **68**, 100502 (2003).
- [10] W. Tabis, B. Yu, I. Bialo, M. Bluschke, T. Kolodziej, A. Kozłowski, E. Blackburn, K. Sen, E. M. Forgan, M. v. Zimmermann, Y. Tang, E. Weschke, B. Vignolle, M. Heping, H. Gretarsson, R. Sutarto, F. He, M. Le Tacon, N. Barišić, G. Yu, and M. Greven, *Physical Review B* **96**, 134510 (2017).
- [11] C. E. Matt, C. G. Fatuzzo, Y. Sassa, M. Månsson, S. Fatale, V. Bitetta, X. Shi, S. Pailhès, M. H. Berntsen, T. Kurosawa, M. Oda, N. Momono, O. J. Lipscombe, S. M. Hayden, J.-Q. Yan, J.-S. Zhou, J. B. Goodenough, S. Pyon, T. Takayama, H. Takagi, L. Patthey, A. Bendouan, E. Razzoli, M. Shi, N. C. Plumb, M. Radovic, M. Grioni, J. Mesot, O. Tjernberg, and J. Chang, *Physical Review B* **92**, 134524 (2015).
- [12] K. Fujita, C. K. Kim, I. Lee, J. Lee, M. H. Hamidian, I. A. Firmo, S. Mukhopadhyay, H. Eisaki, S. Uchida, M. J. Lawler, E.-A. Kim, and J. C. Davis, *Science* **344**, 612 (2014).
- [13] S. Badoux, W. Tabis, F. Laliberté, G. Grissonnanche, B. Vignolle, D. Vignolles, J. Béard, D. A. Bonn, W. N. Hardy, R. Liang, N. Doiron-Leyraud, L. Taillefer, and C. Proust, *Nature* **531**, 210 (2016).
- [14] C. Collignon, S. Badoux, S. A. A. Afshar, B. Michon, F. Laliberté, O. Cyr-Choinière, J.-S. Zhou, S. Licciardello, S. Wiedmann, N. Doiron-Leyraud, and L. Taillefer, *Physical Review B* **95**, 224517 (2017).
- [15] C. Putzke, S. Benhabib, W. Tabis, J. Ayres, Z. Wang, L. Malone, S. Licciardello, J. Lu, T. Kondo, T. Takeuchi, N. E. Hussey, J. R. Cooper, and A. Carrington, arXiv:1909.08102 [cond-mat] (2019), arXiv: 1909.08102.
- [16] B. Michon, A. Ataei, P. Bourgeois-Hope, C. Collignon, S. Li, S. Badoux, A. Gourgout, F. Laliberté, J.-S. Zhou, N. Doiron-Leyraud, and L. Taillefer, *Physical Review X* **8**, 041010 (2018).
- [17] J. Loram, K. Mirza, J. Cooper, and J. Tallon, *Journal of Physics and Chemistry of Solids* **59**, 2091 (1998).
- [18] N. Momono, M. Ido, T. Nakano, M. Oda, Y. Okajima, and K. Kamaya, *Physica C* **233**, 395 (1994).
- [19] N. Barišić, S. Badoux, M. K. Chan, C. Dorow, W. Tabis, B. Vignolle, G. Yu, J. Béard, X. Zhao, C. Proust, and M. Greven, *Nature Physics* **9**, 761 (2013).
- [20] M. K. Chan, N. Harrison, R. D. McDonald, B. J. Ramshaw, K. A. Modic, N. Barišić, and M. Greven, *Nature Communications* **7**, 12244 (2016).
- [21] N. Harrison and S. E. Sebastian, *Physical Review Letters* **106**, 226402 (2011).
- [22] A. Legros, B. Loret, A. Forget, P. Bonnaille, G. Collin, P. Thuéry, A. Sacuto, and D. Colson, *Materials Research Bulletin* **118**, 110479 (2019).
- [23] G. Grissonnanche, O. Cyr-Choinière, F. Laliberté, S. René de Cotret, A. Juneau-Fecteau, S. Dufour-Beauséjour, M. È. Delage, D. LeBoeuf, J. Chang, B. J. Ramshaw, D. A. Bonn, W. N. Hardy, R. Liang, S. Adachi, N. E. Hussey, B. Vignolle, C. Proust, M. Sutherland, S. Krämer, J. H. Park, D. Graf, N. Doiron-Leyraud, and L. Taillefer, *Nature Communications* **5**, 4280 (2014).
- [24] J. Kemper, Ph.D. thesis, Florida State University (2014).
- [25] J. Kačmarčík, I. Vinograd, B. Michon, A. Rydh, A. Demuer, R. Zhou, H. Mayaffre, R. Liang, W. Hardy, D. Bonn, N. Doiron-Leyraud, L. Taillefer, M.-H. Julien, C. Marcenat, and T. Klein, *Physical Review Letters* **121**, 167002 (2018).
- [26] S. E. Sebastian, N. Harrison, M. M. Altarawneh, C. H. Mielke, R. Liang, D. A. Bonn, W. N. Hardy, and G. G. Lonzarich, *PNAS* **105**, 6175 (2010).
- [27] B. J. Ramshaw, S. E. Sebastian, R. D. McDonald, J. Day, B. S. Tan, Z. Zhu, J. B. Betts, R. Liang, D. A. Bonn, W. N. Hardy, and N. Harrison, *Science* **348**, 317 (2015).
- [28] S. Komiya and I. Tsukada, *J. Phys. Conf. Ser.* **150**, 052118 (2009).
- [29] C. Marcenat, A. Demuer, K. Beauvois, B. Michon, A. Grockowiak, R. Liang, W. Hardy, D. A. Bonn, and T. Klein, *Nature Communications* **6**, 7927 (2015).
- [30] S. Blanco-Canosa, A. Frano, E. Schierle, J. Porras, T. Loew, M. Minola, M. Bluschke, E. Weschke, B. Keimer, and M. Le Tacon, *Physical Review B* **90**, 054513 (2014).
- [31] M. Hücker, N. B. Christensen, A. T. Holmes, E. Blackburn, E. M. Forgan, R. Liang, D. A. Bonn, W. N. Hardy, O. Gutowski, M. v. Zimmermann, S. M. Hayden, and J. Chang, *Physical Review B* **90**, 054514 (2014).
- [32] T. P. Croft, C. Lester, M. S. Senn, A. Bombardi, and S. M. Hayden, *Physical Review B* **89**, 224513 (2014).
- [33] T. Niemöller, H. Hunnefeld, T. Frello, N. H. Andersen, N. Ichikawa, S. Uchida, and J. R. Schneider, *Journal of Low Temperature Physics* **177**, 455 (1999).
- [34] J. Fink, V. Soltwisch, J. Geck, E. Schierle, E. Weschke, and B. Büchner, *Physical Review B* **83**, 092503 (2011).
- [35] N. Doiron-Leyraud, S. Lepault, O. Cyr-Choinière, B. Vignolle, G. Grissonnanche, F. Laliberté, J. Chang, N. Barišić, M. K. Chan, L. Ji, X. Zhao, Y. Li, M. Greven, C. Proust, and L. Taillefer, *Physical Review X* **3**, 021019 (2013).
- [36] D. LeBoeuf, N. Doiron-Leyraud, J. Levallois, R. Daou, J.-B. Bonnemaïson, N. E. Hussey, L. Balicas, B. J. Ramshaw, R. Liang, D. A. Bonn, W. N. Hardy, S. Adachi, C. Proust, and L. Taillefer, *Nature* **450**, 533 (2007).
- [37] J. Chang, R. Daou, C. Proust, D. LeBoeuf, N. Doiron-Leyraud, F. Laliberté, B. Pingault, B. J. Ramshaw, R. Liang, D. A. Bonn, W. N. Hardy, H. Takagi, A. B. Antunes, I. Sheikin, K. Behnia, and L. Taillefer, *Physical Review Letters* **104**, 057005 (2010).
- [38] D. LeBoeuf, N. Doiron-Leyraud, B. Vignolle, M. Sutherland, B. J. Ramshaw, J. Levallois, R. Daou, F. Laliberté, O. Cyr-Choinière, J. Chang, Y. J. Jo, L. Balicas, R. Liang, D. A. Bonn, W. N. Hardy, C. Proust, and L. Taillefer, *Physical Review B* **83**, 054506 (2011).
- [39] S. Badoux, S. A. A. Afshar, B. Michon, A. Ouellet, S. Fortier, D. LeBoeuf, T. P. Croft, C. Lester, S. M. Hayden, H. Takagi, K. Yamada, D. Graf, N. Doiron-Leyraud, and L. Taillefer, *Physical Review X* **6**, 021004 (2016).
- [40] Y. Nakamura and S. Uchida, *Physical Review B* **46**, 5841 (1992).
- [41] F. Laliberté, J. Chang, N. Doiron-Leyraud, E. Hassinger, R. Daou, M. Rondeau, B. Ramshaw, R. Liang, D. Bonn, W. Hardy, S. Pyon, T. Takayama, H. Takagi, I. Sheikin, L. Malone, C. Proust, K. Behnia, and L. Taillefer, *Nature Communications* **2**, 432 (2011).
- [42] S. Gerber, H. Jang, H. Nojiri, S. Matsuzawa, H. Yasumura, D. A. Bonn, R. Liang, W. N. Hardy, Z. Islam, A. Mehta, S. Song, M. Sikorski, D. Stefanescu, Y. Feng, S. A. Kivelson, T. P. Devereaux, Z.-X. Shen, C.-C. Kao, W.-S. Lee, D. Zhu, and J.-S. Lee, *Science* **350**, 949

- (2015).
- [43] J. Chang, E. Blackburn, O. Ivashko, A. T. Holmes, N. B. Christensen, M. Hücker, R. Liang, D. A. Bonn, W. N. Hardy, U. Rütt, M. v. Zimmermann, E. M. Forgan, and S. M. Hayden, *Nature Communications* **7**, 11494 (2016).
- [44] J. Chang, C. Niedermayer, R. Gilardi, N. B. Christensen, H. M. Rønnow, D. F. McMorrow, M. Ay, J. Stahn, O. Sobolev, A. Hiess, S. Pailhes, C. Baines, N. Momono, M. Oda, M. Ido, and J. Mesot, *Physical Review B* **78**, 104525 (2008).
- [45] T. Wu, H. Mayaffre, S. Krämer, M. Horvatić, C. Berthier, W. N. Hardy, R. Liang, D. A. Bonn, and M.-H. Julien, *Nature* **477**, 191 (2011).
- [46] A. J. Millis and M. R. Norman, *Physical Review B* **76**, 220503 (2007).
- [47] I. M. Vishik, N. BariÅqiÄĜ, M. K. Chan, Y. Li, D. D. Xia, G. Yu, X. Zhao, W. S. Lee, W. Meevasana, T. P. Devereaux, M. Greven, and Z.-X. Shen, *Physical Review B* **89**, 195141 (2014).
- [48] N. Doiron-Leyraud, C. Proust, D. LeBoeuf, J. Levallois, J.-B. Bonnemaïson, R. Liang, D. A. Bonn, W. N. Hardy, and L. Taillefer, *Nature* **447**, 565 (2007).
- [49] A. Mackenzie, S. Julian, A. Diver, G. Lonzarich, N. Hussey, Y. Maeno, S. Nishizaki, and T. Fujita, *Physica C: Superconductivity* **263**, 510 (1996).
- [50] N. Doiron-Leyraud, S. Badoux, S. René de Cotret, S. Lepault, D. LeBoeuf, F. Laliberté, E. Hassinger, B. J. Ramshaw, D. A. Bonn, W. N. Hardy, R. Liang, J.-H. Park, D. Vignolles, B. Vignolle, L. Taillefer, and C. Proust, *Nature Communications* **6**, 7034 (2015).
- [51] H. Yao, D.-H. Lee, and S. Kivelson, *Physical Review B* **84**, 012507 (2011).